Modeling of Mechanical Alloying: Part I. Deformation, Coalescence, and Fragmentation Mechanisms

D. MAURICE and T.H. COURTNEY

A model of the mechanical alloying process, applicable to a single collision event involving ductile species, is developed. Simple physical models are constructed that allow development of analytical expressions for particle shape and hardness changes during a collision and stipulation of criteria for particle fracture and cold welding. These provide a "snapshot" of that which transpires during a single collision event. The model also accounts for the heterogeneity of deformation within the powder trapped between colliding media. This heterogeneity, together with the model criteria, can then be incorporated within a computational scheme capable of predictive description of the evolution of powder morphology and properties during mechanical alloying, as will be described in a subsequent article.

I. INTRODUCTION

MODELING of complex materials processing schemes has been a subject of recent research. Examples include sintering,[1] hot isostatic pressing (HIPing),[2] liquid infiltration of fiber composites,[3] rapid solidification,[4] and welding.[5,6] If the parameters controlling a process can be identified, are few in number, and do not interact significantly, analytical expressions can often be developed to describe parametric effects. These can then be integrated into a suitable computational scheme that ultimately describes process behavior or efficiency. Sintering diagrams predicting neck development and densification progression provide an example of this type of modeling.[7] Refinements of simple models, or analyses of more complex processes having a large number of important process parameters or properties devolving on these, require numerical simulation from the outset. Good examples are recently developed algorithms for mimicking HIPing.[8]

Models developed for complex processes cannot be expected to be absolutely precise. Rather, they are intended to identify important parameters, define the functional dependence of the process output (*e.g.*, density and grain size for HIPing) on process variables, and predict results with an acceptable level of precision. One useful result of such process modeling is considerable reduction in the empirical studies needed to refine a process into a useful engineering tool. In this series of articles we summarize some recent efforts, carried out in this vein, to model mechanical alloying (MA). Our efforts have focused on the mechanics of the process, with particular emphasis on MA of ductile metals. This first article develops equations useful for delineating how particle shape, hardness, and size change during milling of ductile metals. Particle size depends on the frequencies of particle welding and fracture events during alloying. Criteria for these are presented. The resultant equations provide an analytical basis for describing MA. To be useful, however, they must be incorporated into a numerical computational scheme. Subsequent articles synopsize two programs developed for this purpose. In addition, the computational approach is applied to results of previous experimental studies.

In MA, a powder charge is placed in a high-energy mill, along with a suitable grinding medium. Powder trapped between colliding balls is subject to deformation, as well as to potential coalescence and/or fragmentation. These are the sources of the evolution of powder morphology and size; the relative rates with which the events take place control microstructural development. The product powder influences the properties of subsequently consolidated products. Thus, it is desirable to predict and control development of the structure of milled powders.

Aspects of the events that occur during MA have been known for some time and have been described qualitatively.[9,10] In brief, malleable powder particles entrapped between colliding media are subjected to extensive plastic deformation. They consequently harden, sometimes considerably. In the first MA stages, particle flattening is concurrent with this deformation. Particles also cold-weld to each other during impaction, and they sometimes fracture as well; indeed, a proper balance between the fracturing and welding frequencies is usually required for successful alloying. The powder coalescent and fracture events also alter powder particle shape. Finally, the repetitive particle kneading associated with deformation, coalescence, and fracture processes produces significant microstructural refinement. The modeling we have conducted is concerned with predicting the temporal evolution of the microstructural and mechanical characteristics of powder during MA.

Modeling of MA is complex and multifaceted, involving concepts of mechanics, mechanical behavior, heat flow, thermodynamics, and kinetics. Despite, and perhaps because of, this complexity, modeling of the process has been of recent interest.[11–22] Modeling approaches can be classified as either local or global. Local

D. MAURICE, formerly Graduate Student, Department of Materials Science and Engineering, University of Virginia, Charlottesville, VA, is currently Research Fellow, Department of Mechanical and Materials Engineering, University of Western Australia, Nedlands, Australia. T.H. COURTNEY, formerly Professor, Department of Materials Science and Engineering, University of Virginia, is currently Professor and Chair, Department of Metallurgical and Materials Engineering, Michigan Technological University, Houghton, MI.

Manuscript submitted April 9, 1993.

modeling describes the various effects (thermal and mechanical) and events (deformation, fracture, and welding) that transpire when powder particles are entrapped between colliding or sliding surfaces.[11–13,15–19] Thus, local modeling is generic in that parameters that affect the various events—such as impact velocity, angle of impact between colliding workpieces, charge ratio, *etc.*—are common to all devices, although the values of some of the parameters (*e.g.*, impact velocity) are specific to a particular type of mill and its operating conditions. Global modeling is device-specific. For example, this type of modeling considers factors such as the distribution of impact angles and the heterogeneity of powder distribution within the mill[12,14,18]—factors which clearly differ from one type of device to another.

This article provides a compendium of our recent research on MA at the local level. It focuses on the basic physics of the deformation, fracture, and welding events. The derivations presented attempt to define the parametric dependencies of these, and thus the numerical factors provided are only approximate. Readers desiring more details are referred to Reference 21.

While MA provides a means for developing novel microstructures, there is nothing sophisticated about the manner by which this is accomplished. Mechanical alloying is essentially a deformation process taking place on a small scale. It is this scale which makes possible novel microstructures; the scale also makes difficult the determination of that which transpires during an impact between grinding media. However, we can speculate on the deformation and other events that take place, as described in the following sections.

II. COLLISION GEOMETRY

Regardless of the mill used, MA is characterized by collisions between tool and powder. There are several possible geometries for such collisions. For example, powder may be trapped between two colliding balls or caught between a ball and the container wall. In the case of an attritor, powder may be impacted between the grinding media and the rotating impellers. From a geometrical standpoint, however, it is clear that the greatest number of collisions are of the ball-powder-ball type. For this reason, we restrict our discussion to this type of collision, recognizing that geometrical differences associated with other types of collisions can be accounted for fairly easily.[11]

Rolling (sliding) of balls is commonplace in attritors and horizontal ball mills. However, Rydin *et al.*[14] have presented evidence suggesting that such events do not contribute significantly to powder plastic deformation, and hence to coalescence and fragmentation, in attritors. As a consequence, rolling and sliding events between balls are not considered in this article, which focuses on laboratory mills; the pertinence of these events to large commercial mills requires examination of the global mechanics of such mills.

We begin by examining how certain variables—specifically, powder shape and hardness—affect a single collision. The degree of powder deformation that occurs during an impact is obviously a function of powder hardness, and it will be seen later that hardness also influences coalescence behavior. Particle shape enters into aspects of both coalescence and fracture.

Another characteristic of MA is that the extent of deformation the powder experiences depends on the amount of powder involved in a collision. To estimate this quantity, we previously proposed a "sweeping" mechanism[11] by which balls are coated with a thin layer of powder as they move between collisions. In addition, other workers have estimated this thickness in an empirical manner.[23,24] Both approaches yield reasonable agreement with experimental results,[11] and in many of the applications described in the second article of this series, we accept that the coating thickness is on the order of 100 μm, a value consistent with the studies mentioned. However, the coating thickness can be conveniently changed in the programs described therein.

A second potential influence on the outcome of a collision is the shape of the powder particles involved in it. Initial powder shape can vary from spherical to flake, and particle shape also varies during processing. We model the shape of a particle as an oblate spheroid. The shape is then characterized by a ratio: that of the minor to the major axis of the spheroid (Figure 1). In later sections, we explore how deformation, fragmentation, and coalescence change the shape factor, as well as how these processes depend on it.

Deformation necessarily changes particle shape. The nature and extent of such changes depend on both the extent of deformation and the deformation "direction." This direction in turn depends on the orientation of the particle with respect to the direction of impact a colliding ball makes with it. We assume that particles rest on a grinding ball with their major axes parallel to the ball's surface (Figure 2). This orientation is consistent with the sweeping mechanism, satisfies the requirement of lowest potential energy, and recognizes the effects of adhesive forces. Potentially hundreds to thousands of particles may be present on a ball at the time of impact; although in reality their orientations will vary, we consider all to be aligned as just described.

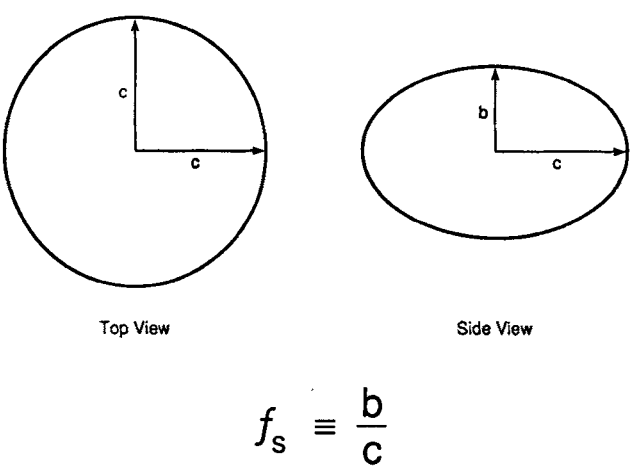

Fig. 1—Powder particles with shapes ranging from spherical to disk shaped can be modeled as oblate spheroids. The shape is characterized by the factor f_s, which is equal to b/c, where b is the minor axis and c is the major axis of the particle.

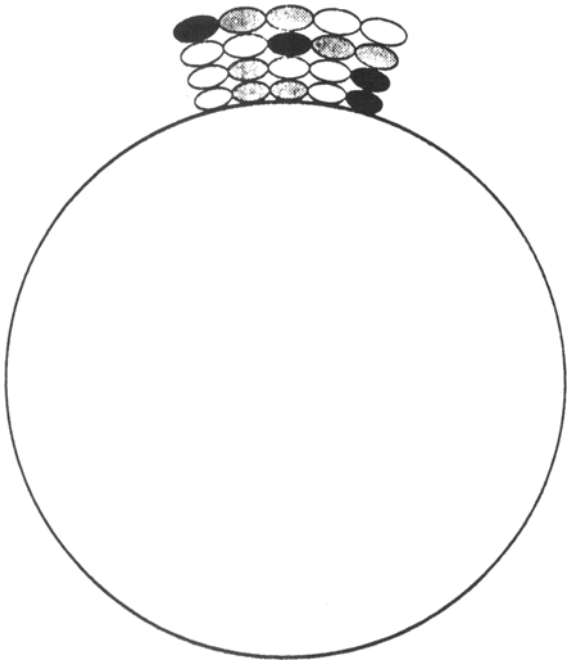

Fig. 2—Individual powder particles are assumed oriented so that the major axis of the particle lies parallel to the ball's surface. Rationales for this assumption are provided in the text. An assemblage of such particles (not to scale) is depicted. The differently shaded particles represent different species.

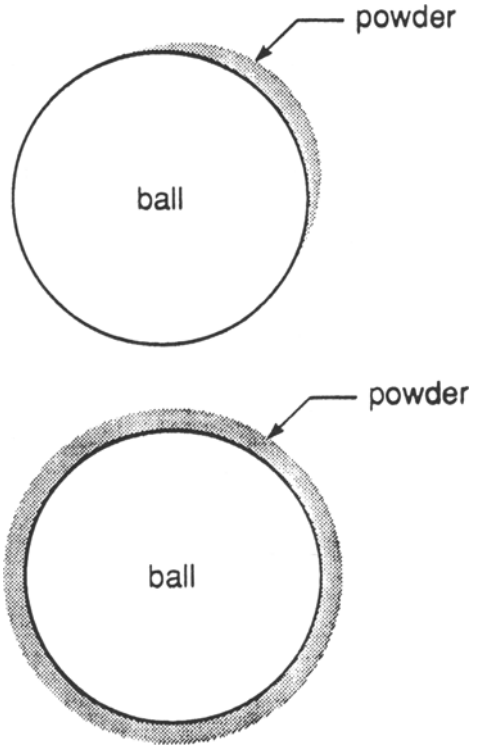

Fig. 3—Grinding balls are typically not uniformly coated with powder, as indicated on the top. However, analysis of the mechanical response of an impact is simplified by doing so. Thus, as shown on the bottom, a ball and its associated coating are considered to constitute a composite ball, which is used to model the mechanical response.

We will refer to a grinding ball and its associated coating as a composite ball (Figure 3). Although grinding balls are not uniformly coated with powder, analysis of the mechanical response to an impact is simplified by assuming this to be so. As the effect of the impact is restricted to only a very small fraction of the ball's surface, this choice of geometry has little effect on results obtained.

III. DEFORMATION DURING THE COLLISION

Powder entrapped between balls undergoes deformation. The degree of this deformation largely determines coalescence and fragmentation proclivities during impact, and the degree may be determined by modeling a collision in stages that allow apportionment of deformation between the balls and the powder on their surfaces.

The kinetic energy of the balls is converted to deformation energy during the approach of their centers (Figure 4). The stress homologous to this energy conversion is the materials' resistance to elastic and plastic deformation. For the powder (much of which plastically deforms), this resistance is taken as that of the softer material present when milling of two-phase materials is considered. To plastically deform harder material requires that the softer species be work-hardened to a flow stress equivalent to that of the harder one. It will be seen later that this delays, and in certain instances may limit, the occurrence of welding and fracture of some particles. In our model, the grinding media are assumed to be harder than all powders present during processing. Thus, the media experience only elastic deformation during impact. In practice, however, some powders may well attain the hardness of the media; this aspect of the model, then, would benefit from further refinement.

We also invoke the average strain theorem, which states that the average state of strain in a given volume element is determined from the deformations applied to its boundaries. The result of this assumption is that we may treat all particles *of a given species* at a *given distance from the center of contact* as undergoing the same deformation. In a similar vein we apply the average stress theorem, which equivalently states that the average stress in a volume element is equal to the tractions applied to its boundaries. What these theorems imply for our purpose is that essentially all particles of a species that are located on a line between homologous points on colliding balls (for example, their centers) experience the same average stress and strain. Thus, for example, the average state of stress between powder particles (*at a given position in the contacting region of the balls*) is the same as that between the colliding balls.

A ball and adhering powder constitute a composite ball. A magnified view (Figure 2) schematically shows how powders of different species might aggregate. Although the arrangement is idealized, it is statistically correct in that some fraction of each powder species resides in each "column." We take the response of each species to be that of an individual (fully dense) particle, rather than that of a porous body. We justify this by

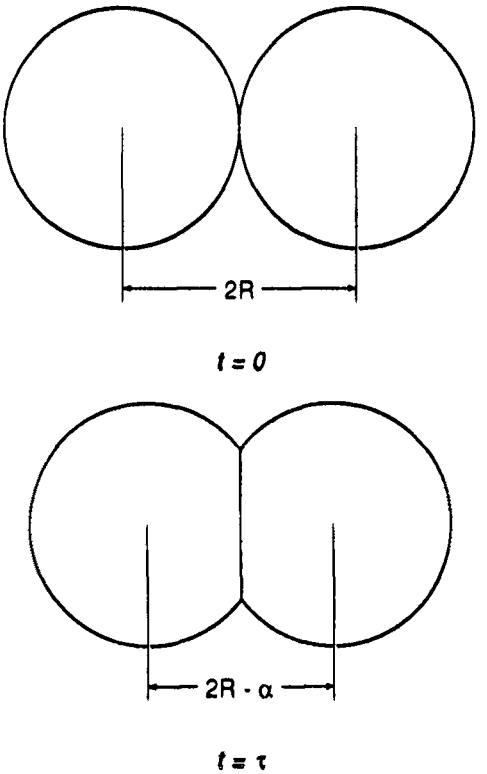

Fig. 4—When composite balls collide, their kinetic energies are converted into deformation energy. This is manifested by a decrease in their center-to-center spacing (equal to $2R$ at contact initiation) by the distance α (at the end of the compression phase of impact). The actual contact radius, relative to the ball radius, is highly exaggerated in this figure.

noting that the true plastic strains the powder experiences during an impact are much greater than the strain associated with densification during uniaxial compression.[25]

The presence of species of different hardnesses results in the necessity of modeling a collision in stages, with the softer species deforming first. In the initial stages of impaction, both powder and balls deform elastically. The distribution of stress over the contact area is shown schematically in Figure 5. On further approach of the ball centers, the stress at the contact center attains the powder hardness. With further deformation, this stress is reached over a finite radius, the radius increasing with time of contact. Outside this radius, the stress distribution is the same as it would be in an elastic collision. As mentioned, balls are assumed sufficiently hard so as to not plastically deform during impact.

Collisions between balls are modeled on the basis of this reasoning; the model is developed in detail in Appendix A. It should be noted that for a different collision geometry (*e.g.*, ball-container wall), the stages of the collision do not change, and we would expect the results to differ only by a geometrical factor of order unity. Other minor limitations of the model are discussed in Appendix A.

One important result is that, for most collisions, the first stage (during which both the ball and the powder deform elastically) is very short in comparison with the total time of collision. Most of the approach between

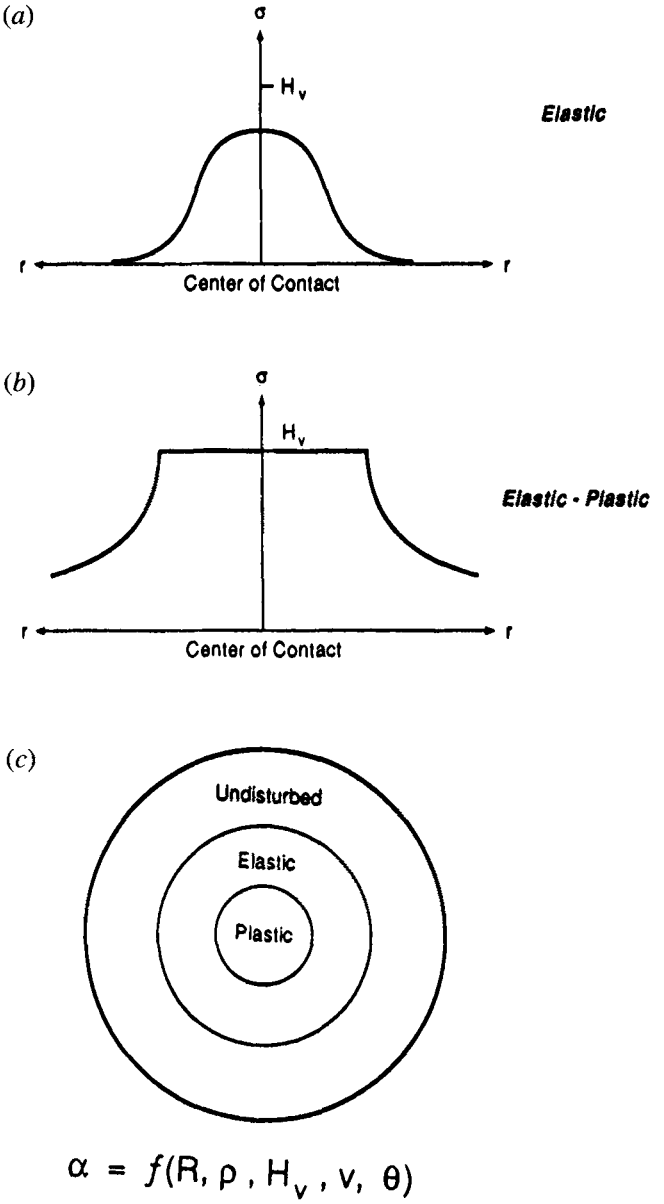

Fig. 5—Schematic of the distribution of stress over the contact area during a collision between composite balls. (*a*) Early in the collision, the balls deform elastically. (*b*) The powder begins to deform plastically when the stress attains the powder hardness. (*c*) During this stage, the center of the contact area is characterized by plastic deformation of the powder, the annulus around it by elastic deformation of both powder and ball, and outside this annulus there is no deformation of either (not to scale).

two balls is associated with plastic deformation of the powder. The approach (Figure 4), and hence deformation, may be expressed as a function of radius within the contact area as

$$\alpha(r) = Rv\left(\frac{\rho_b}{H_v}\right)^{1/2} - \frac{r^2}{R} \qquad [1]$$

where r is the distance from the center of contact, R the radius of the balls, v the relative velocity of the balls at impact, ρ_b the density of the grinding balls, and H_v the powder hardness. As written here, Eq. [1] ignores factors of order unity and the effect of impact angle of the

colliding balls. These considerations are accounted for in the more complete treatment presented in Reference 21, where arguments are made for considering only low-angle (almost "head-on") collisions, implicit in Eq. [1]. Congruous with this position, we disregard high-angle (glancing) impacts in the model development, although we will acknowledge the effects of other than direct impacts where appropriate. We note that the analysis applies only when some minimum quantity of powder coats the balls. Should the approach, as predicted by Eq. [1], exceed the coating thickness, or should the hardness of the powder reach that of the grinding media, this description must be modified.

Having established a protocol for determining the deformation of the powder charge, we now investigate the manifestations of this deformation on powder particle hardness, coalescence, fragmentation, size, and shape. The analytical expressions developed form the basis of the numerical scheme described in Part II.

IV. POWDER HARDNESS

Powder hardness is an important process parameter in that it affects the degree of powder deformation during impact and determines the normal elastic force acting to separate particles during welding. Hardness also affects the time interval between successive impacts of a particle, as discussed later.

There is a dearth of constitutive relations for metals valid over the wide range of strains to which they are typically subjected during MA. As a consequence, we use a simple plastic constitutive relation commonly applied over *lesser* strain ranges, *i.e.*,

$$\sigma_y = \sigma_{y0} + K\varepsilon^n \qquad [2]$$

where K is the strength coefficient, n the work-hardening exponent, σ_y the flow stress at the accumulated plastic strain ε, and σ_{y0} the initial flow stress. On using $H_v = 3\sigma_y$, we have

$$H_v = H_{v0} + 3K\varepsilon^n \qquad [3]$$

The strain is determined from

$$\varepsilon = -\ln\left\{\frac{h_0 - \alpha(r)}{h_0}\right\} \qquad [4]$$

where $\alpha(r)$ is the approach (*cf.* Eq. [1]) and h_0 the powder coating thickness. It is thus straightforward to determine strain as a function of radial position within the contact zone. With the aid of computational techniques, the strain (and the hardness) resulting from a series of impacts can also be monitored.

As noted, one difficulty in applying these equations stems from the paucity of work-hardening exponent and strength coefficient data over the wide range of strains, strain rates, *etc.*, to which powder particles are subjected during MA. Additional errors could arise from our neglect of temperature and strain-rate effects (although the two factors tend to cancel) on material hardness and of the changes in hardening rate (Stage IV hardening)[26] at the very large strains endemic to MA. As such data become more available, the model and its computational application can be modified accordingly.

V. COALESCENCE MECHANISMS

Cold pressure welding has been the subject of considerable quantitative study.[27–33] However, it is described only qualitatively in the MA literature. That description may be encapsulated as follows. As colliding balls plastically deform powder particles, their contaminant films (typically oxides) rupture, exposing underlying metal. When the free metal surfaces of the particles come into contact, a bond is formed. In this section, we apply these underlying physics and use results of previous work[27–29,31] to develop relations that predict the conditions for formation of a weld.

The oxide layer on the particles is assumed to be brittle and to fracture at the onset of plastic deformation of the underlying metal. A consequence of assuming such brittle behavior is that the area of the contaminant film remains constant. However, as the particles flatten in compression, their surface area increases and underlying metal is progressively exposed. If S_i and S_f are respectively defined as the particle pre- and post-deformation surface areas, the particle surface area can be determined at any stage of deformation *via* consideration of the powder shape as an oblate spheroid. The minor axis is reduced and the major axis increased by deformation; the extent of these changes and the associated surface-area changes can be determined as shown in Section VII. The area of the oxide layer is equal to S_i, and the area of the exposed metal is equal to the difference between the post- and pre-deformation areas ($\Delta S = S_f - S_i$). The fractional metallic area exposed is $\Delta S/S_f$.

Two such particles in contact generally do not have complete overlapping of their exposed metal surfaces. The statistically averaged fractional matching area on two particles varies with the square of the exposed fractional area. Thus, the actual fractional matching area can be written as $J(\Delta S/S_f)^2$, where J is a proportionality constant. Mohamed and Washburn[30] found that J lies between 0.7 and 0.8 over a wide range of deformation. We use $J = 0.75$ as a reasonable estimate for our analysis.

Welding is assumed to take place only in the region over which intimate metal-metal contact is established *via* plastic deformation. This area may be reduced if any dispersoids (*i.e.*, nondeforming inclusions having a size much less than the particle size) are present between the particles. Then the area of metal-to-metal contact is

$$A_w = \pi r_p^2\left[J\left(\frac{\Delta S}{S_f}\right)^2 - n_d\left(\frac{r_d^2}{r_p^2}\right)\right] \qquad [5]$$

where n_d is the number of dispersoids trapped in the potential weld region of radius r_p, and r_d is the radius of the (presumed spherical) dispersoids. The force require to separate the weld that forms is

$$F_w = A_w\sigma_u \qquad [6]$$

where σ_u is the tensile strength of the weld. For two adhering particles of the same material, we take this

strength as the tensile strength of the bulk material. For two welded particles of different materials, the weld strength is assumed to be the lesser of the tensile strengths of the different materials. When a cold weld is made between two lamellar particles (*i.e.*, composite particles containing two species), weld strength is taken as a "rule of mixtures" strength on the basis that the weld is a mixture of similar and dissimilar metal bonds.

Two interesting points emerge from this description. The first is that the necessity of having exposed metal surface on both particles implies that both particles must deform plastically before welding between them can take place. Thus, in a system of two species having disparate starting hardnesses, welding is delayed until the hardnesses of both are equal. As a corollary, there are thus two ways in which a composite particle can be formed. If particles of the two species are of equal hardness, they may weld directly according to the description just presented; we term this an "A–A" weld (Figure 6(a)). If they are of differing hardnesses and the harder particle is (considerably?) smaller than the softer one, hard particles may be encapsulated in the softer species; we call this "A–B–A" welding (Figure 6(b)). (Note that deformation constraints might lead to deformation of the harder particle once it is incorporated into the softer one; this point is considered in detail in Reference 21.) These two cases form the bases of two predictive programs designed to handle welding events in MA, which are elaborated on in Part II of this series. Each program considers just one of these weld mechanisms. A future refinement might be to have the program test for, and specify, the operative weld mechanism.

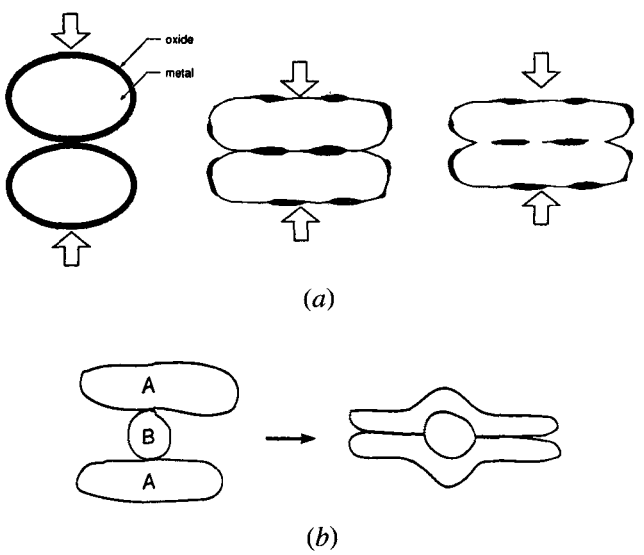

Fig. 6—Two different forms of coalescence during mechanical alloying. (*a*) Coalescence effected by cold welding, termed an A–A weld even if the particles are different species. As the two particles, of equal or comparable hardness, are pressed together, their surface area increases; their brittle oxide layer fractures, exposing clean metal surface; and, when the metal surfaces come in contact, a metal bond is formed. (*b*) Coalescence effected by particle encapsulation (A–B–A welding). When a hard dispersoid is trapped between deforming particles, bonding by encapsulation is possible. If following entrapment the composite particle is deformed sufficiently, a true bond may form between the ductile materials and the dispersoid.

Elastic recovery forces (arising from particle deformation) and shear forces (resulting from any relative tangential motion of the colliding balls, Figure 7) act to separate welded particles and sever the juncture between them. The elastic recovery forces act in an annulus about the plastic deformation zone. If dispersoids are trapped between powder particles, an elastic recovery force acts through them as well. The total elastic recovery force is given by

$$N_e = \pi r_p^2 H_v \left[\frac{n_d r_d^2}{r_p^2} + \frac{\pi^4}{6(1 + 1.33 \tan^2 \theta)^{0.5}} \left(\frac{R_p^2}{r_p^2} \right) \delta^2 H_v^2 \right] \quad [7]$$

where $\delta = (1 - \nu^2)/E$, and R_p is the particle's volume effective radius, θ the relative impact angle (see Figure A1), ν the particle's Poisson's ratio, and E its elastic modulus. The second term in parentheses represents the elastic response of the annulus around the plastic zone. The average shear force acting over the weld surface is

$$T_b = \pi r_p^2 H_v \left(\frac{0.44 \tan^2 \theta}{1 + 1.33 \tan^2 \theta} \right)^{0.5} \quad [8]$$

Appendix A also presents the development of the elastic response as well as shear force of Eq. [8].

An effective stress argument is applied as a success/failure criterion for the weld. If the following condition is met, the particles remain welded; if not, they separate:

$$F_w^2 \geq N_e^2 + 3T_b^2 \quad [9]$$

If particles separate, the possibility remains that they may exchange metal through adhesion. The criterion for this case has not been developed.

The effect of surface reoxidation—for example, when a mill operates in air—can also be included in the model. Powder particles typically have an oxide coating of 2 to 10 nm.[34,35] As this is just several atomic layers thick, we assume that oxide reforms as islands, rather

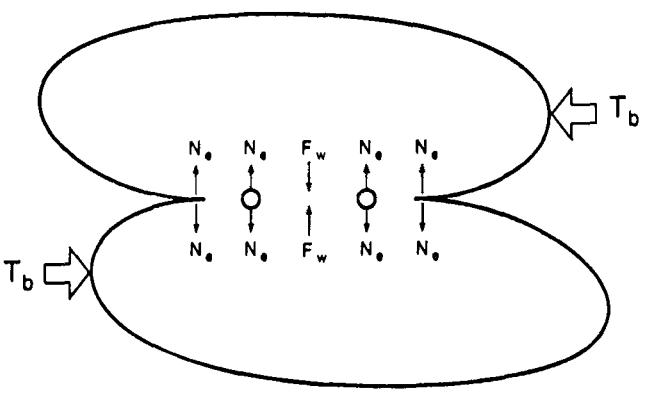

Fig. 7—The newly formed bond between welded particles is subjected to forces acting to sever the weld as the grinding media balls separate. Elastic recovery forces (N_θ) act to separate the particles in the annulus around the weld area and through any trapped dispersoids. A tangential component of motion between the balls (T_b) tends to shear the weld between the particles. The strength of the weld (F_w) must be greater than the effective stress of these separation forces for the bond to be maintained.

than coating the entire particle. That is, the oxide is treated in terms of surface coverage rather than thickness. This allows us to determine the amount of exposed metal surface prone to reoxidation during processing. The fractional metal surface exposed is reduced by reoxidation; the reduction is represented by the second term in the following equation:

$$Z_i = \left(\frac{\Delta S}{S_f}\right)_i - \zeta \frac{Z_{i-1}}{(\Delta S/S_f)_i} \qquad [10]$$

In Eq. [10], $(\Delta S/S_f)_i$ is the fraction of surface exposed through cumulative deformation through impact i, and ζ is the fraction coated during the interval between relevant impacts (we show later how this interval is calculated). Based on the work of Tylecote *et al.*,[36] it is reasonable to assume that any oxide layer attains full coverage in approximately 20 minutes (in air). So, for example, if the time between relevant impacts is 2 minutes, the factor ζ in Eq. [10] is 0.1. While the programs described in Part II are developed to predict results of welding in an inert atmosphere, as discussed here they can be expanded to include welding in an atmosphere containing oxygen.

We assume that a particle welds only once during impact and to only one other particle. Although more welding events may happen, this deviation would only result in a numerical error when "counting" particles as described in the second part of this series. As will become apparent, any error introduced in this way does not much affect the accuracy of model predictions. We also note that while the shapes of particles that have welded are changed, the shape can still be described in terms of an oblate spheroid.

VI. FRAGMENTATION MECHANISMS

We have considered three possible mechanisms of particle fragmentation during MA. The first, forging fracture (Figure 8(a)), may develop over several impacts. Cracks formed in this way grow radially along the major axes of the particles. The second type of fracture considered is termed shear fracture (Figure 8(b)). This fragmentation mode is characterized by cracks running perpendicular to the particle's minor axis. As a result of crack closure forces, this mechanism is likely not operational in MA.[21] A third type of fragmentation is dynamic fracture (Figure 8(c)). This requires strain rates higher than those characteristic of common MA devices, but may occur in some of the higher-energy mills during impacts characterized by high collision velocities and/or minimal powder coatings. The collision analysis used in our model cannot be applied under these conditions. Our discussion of fracture is limited to those events we consider pervasive in the more common laboratory and commercial mills, and is thus restricted to the fracture depicted in Figure 8(a).

Crack initiation is a precursor to forging fracture. We assume that a crack initiates when a critical tensile strain is attained and that the initial crack length is equal to the distance over which that threshold strain is exceeded. Subsequent crack propagation occurs when the plastic energy release rate exceeds a value characteristic of the material. This requires that the crack exceed a certain length. If the particle is sufficiently small so that this length is greater than the particle size, the particle is considered below its comminution limit and will not fracture.

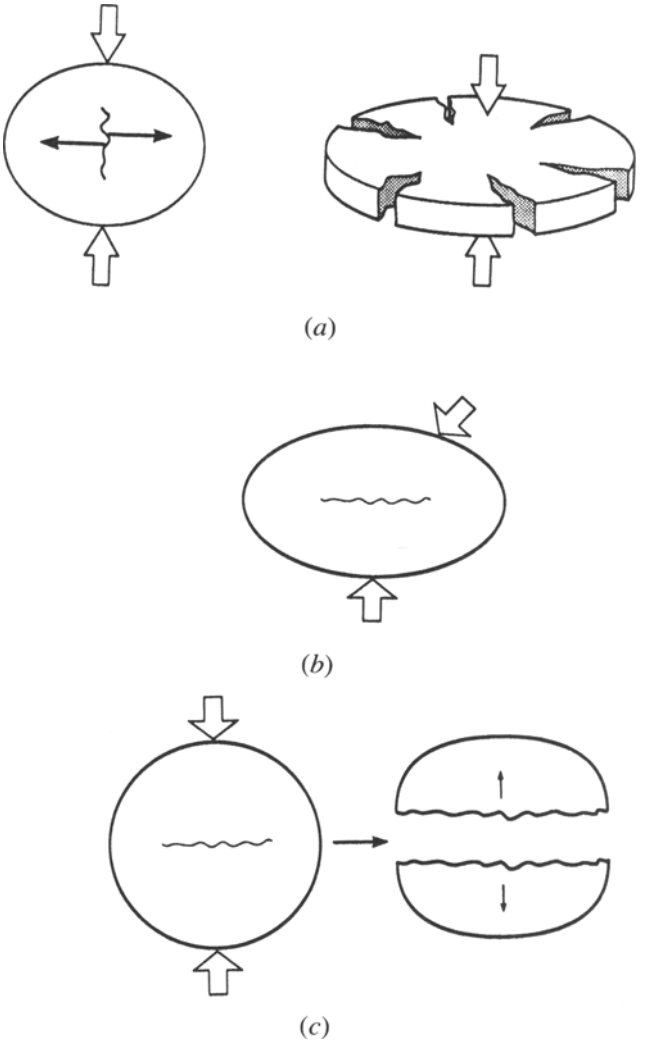

Fig. 8—Three possible fracture modes taking place during MA. (*a*) Forging fracture is the fragmentation mechanism most likely to occur. Edge cracks are formed (perhaps over several impacts) along the particle circumference and grow along the particle axis. This is a microscopic version of fractures that take place in macroscopic forgings. (*b*) Shear fracture, in which cracks run perpendicular to the particle's minor axis, is not as likely to occur due to crack closure forces. (*c*) Dynamic fracture, in which separation is effected by a reflected tensile wave, requires strain rates higher than those characteristic of most MA devices.

It is thus necessary to determine the location and directions of tensile strains in a compressed body. We considered two methods of determination. The first, based on work of Avitzur,[37] incorporates the concepts of sticking friction at the tool-workpiece interface and of barrelling. Strain is greatest at the outer circumference, and there is a dead metal zone at the contact center. This method predicts crack initiation at the outer circumference of the particle; based on studies of forging failure of ductile materials,[38,39] this seems most plausible. In the second method, we disregard the presence of a dead

metal zone and compute strain as a function of position based on theoretical considerations (Appendix B). Strain is greatest at the contact center and decreases with radial distance from this point. This predicts crack initiation in the particle center, as would be expected for a brittle material. While the first method is more plausible with respect to the conditions and materials of MA, there is little difference in the criteria for crack initiation or final fracture between the two approaches. As the second method results in a more general solution, it is used in the model. We proceed with the knowledge that the location of crack initiation is less plausible with this choice, but that the results of the two methods are sufficiently close to justify method selection on the basis of tractability.

To predict fracture we must first determine strain distribution. This is done by considering powder particles as oblate spheroids. An individual spheroid, in turn, can be imagined as constituting a series of nested, concentric cylinders of differential thickness. The innermost cylinder has a height equal to the particle's minor axis and a radius approaching zero; the outermost cylinder has a height tending to zero and a radius equal to the spheroid major semiaxis. These differential cylinders are sequentially compressed as powder is deformed. A cylinder under axial compression experiences equal tensile strains in the radial and circumferential directions. It is most convenient to work with axial strain, since that is immediately determined from the approach at impact. For a cylinder under axial compression (and no barreling), we have

$$\varepsilon_\theta = -0.5\varepsilon_z \qquad [11]$$

where ε_θ and ε_z are the circumferential and axial strains, respectively. In Appendix B, we determine the plastic deformation of a powder particle as a function of radial position within the particle, so that the axial (and hence circumferential) strain can be determined. Crack initiation (and growth) is assumed to occur for the condition $\varepsilon_\theta = \varepsilon_f$, where ε_f is the tensile true fracture strain. For ductile materials, the requirement for initiation/growth at some distance r from the center of contact between two particles becomes

$$\varepsilon_z(r) = -2\varepsilon_f \qquad [12]$$

A similar analysis can be carried out for brittle materials. In this case, the requirement for initiation/growth is

$$\varepsilon_z(r) = -\frac{1}{\nu}\varepsilon_f \qquad [13]$$

We now apply this to predict fracture strain of a powder particle. Due to the small size of powder particles, linear elastic fracture mechanics cannot be applied; rather, an elastic-plastic analysis is necessary. Crack length is assumed equal to the distance over which a critical strain, discussed earlier, is exceeded. When the crack reaches a critical length, determined by the critical value of the J integral, it propagates catastrophically. The value of the J integral is approximated by[40]

$$J = \beta\sigma_0\varepsilon_0 a\pi\sqrt{m}\left(\frac{\sqrt{3}\sigma}{2\sigma_0}\right)^{m+1} \qquad [14]$$

where $\beta = (1/\varepsilon_0)(\sigma_0/K)^m$, with K being the strength coefficient and $m = 1/n$ (n is the work-hardening coefficient). The critical J value (J_{Ic}) is related to the critical stress-intensity factor, K_{Ic}, through[41] $J_{Ic} = K_{Ic}^2/E$. The critical crack length (a_c) is obtained for $J = J_{Ic}$ or

$$a_c = J_{Ic}\frac{K^m}{\pi\sqrt{m}}\left(\frac{2}{\sqrt{3}\sigma_u}\right)^{m+1} \qquad [15]$$

In the programs described in Part II, values of J_{Ic} and a_c are calculated based on input values of the material parameters K_{Ic}, E, K, σ_u, and n.

Using the expression for strain as a function of radial position within the powder particle permits determination of the total approach between balls needed in order to exceed some critical strain over a given length. The condition for forging fracture is now expressed as

$$\frac{\alpha(r)}{h_0} = 1 - \left(1 - \frac{a_c^2 f_s^{2/3}}{4R_p^2}\right)^{0.5}\exp(-\varepsilon_c) \qquad [16]$$

where ε_c is the critical strain to fracture (*cf.* Eqs. [12] and [13]). The factor of 4 in the denominator of the last term on the right-hand side of Eq. [16] stems from the radial symmetry of the particles; to exceed the critical strain over a_c requires that the strain be exceeded over a radial distance one-half of a_c.

Maintaining geometrical similitude, fragmented particles are still oblate spheroids, although their shape factors are changed due to fracture. We also assume that a particle fractures only once, and then into two pieces, during an impact. It is quite possible for a particle to break into more than two pieces when fractured. This would introduce a counting error similar to that described previously for coalescence events and has a similar associated (but fairly minimal) error.

VII. SHAPE FACTOR

Particle shape may affect coalescence and fragmentation events. Moreover, particle shapes are altered by these occurrences as well as by plastic deformation. This section provides details of shape modeling and shape changes during processing.

Most particle shapes, with the exception of needles, may be reasonably described as oblate spheroids (Figure 1). The major semiaxis is c; the minor semiaxis, which also defines the axis of revolution, is b. The shape factor is defined as $f_s = b/c$. The volume of an oblate spheroid is

$$V_c = \frac{4\pi}{3}c^2 b \qquad [17]$$

A volume equivalent radius of the spheroid can be defined as $R_p = (c^2 b)^{1/3}$, and both semiaxes may be expressed in terms of this radius and the shape factor.

$$b = R_p f_s^{2/3} \qquad c = R_p f_s^{-1/3} \qquad [18]$$

Recall that particles on ball surfaces are assumed to have their major axes parallel to the surfaces and the minor axes perpendicular to them. The minor axis is reduced,

and the major axis increased, as a particle is compressed. Knowing that particle volume is conserved during deformation, the shape factor after deformation can be expressed as

$$f_{sf} = \left(\frac{b_f}{b_i}\right)^{1.5} f_{si} \quad [19]$$

where the subscripts i and f denote the pre- and post-deformation shape factors, respectively. The change in the minor axis dimension can be related to powder deformation:

$$\frac{b_f}{b_i} = 1 - \frac{\alpha(r)}{h_0} \quad [20]$$

Thus, the shape factor can be expressed in terms of bulk deformation:

$$f_{sf} = \left(1 - \frac{\alpha(r)}{h_0}\right)^{1.5} f_{si} \quad [21]$$

In the case of a weld event between two particles, the minor axis of the new particle is taken as the sum of the minor axes of the original two (unless the sum is greater than the major axis, in which case the major and minor axes are then reversed). For the programs detailed in the second part of this series, if the two powders are of different species, the minor axis of the composite particle formed is equal to the sum of the minor axes of the particles of the different species, and the major axis is set equal to the greater of their major axes. Similarly, in the case of forging fracture, the major axis is halved, again doubling the shape factor (unless the resulting major axis is now less than the minor axis, in which case the axes are reversed). As both weld and fracture events take place after some deformation, the final shape factor is a multiple of the shape factor after deformation, determined on the basis of the events the particle experiences.

The surface area of a particle is also altered by deformation, fracture, and coalescence. Surface area affects the proclivity for welding, as discussed earlier. Surface-area changes during deformation can be calculated at any stage of deformation using

$$S = \frac{\pi R_p^2}{f_s^{2/3}}\left[2 + \frac{f_s^2}{e}\ln\left(\frac{1+e}{1-e}\right)\right] \quad [22]$$

where $e = (1 - f_s^2)^{1/2}$.

VIII. SUMMARY

In this article we have presented simplified models describing changes in powder particle shape and hardness during MA. We have likewise defined criteria for particle welding and fragmentation, and have noted how these alter particle shape. The equations presented are of the "snapshot" variety. That is, they are applicable only for a specific impact event. Because particle properties, size, and shape vary continuously during MA, in order for these formulations to be useful for predictive purposes they must be incorporated into a computational scheme. In subsequent articles, we describe the schemes we have developed and some applications of the programs.

APPENDIX A: COLLISION MECHANICS

In this section we analyze the mechanics of a collision between balls. The method parallels those of Andrews[42] and Maw.[43]

Consider two balls colliding at some relative velocity and impact angle, as depicted in Figure A1. To a first approximation we can write

$$N = F\cos\theta_i \quad [A1]$$

where F is the force developed during the collision as a result of the resistance of the composite ball to deformation, N is the normal component of that force, and θ_i is the initial angle of impact. The tangential component of the force is

$$T = \left[\frac{2(1-\nu)}{2-\nu}\right] F\sin\theta_i \quad [A2]$$

where the term in brackets arises from the ratio of normal to tangential compliance.[44] Designating this term as C, we have

$$T = CN\tan\theta_i \quad [A3]$$

Equations [A1] through [A3] apply for collision angles below which gross slip between the colliding balls occurs. For such slip, the entire contact area of one ball slides on that of the other ball. In these circumstances, $\tan\theta_i$ in the equations must be replaced by μ, the coefficient of friction. In this Appendix, however, we consider the collision to take place under "sticking" conditions, *i.e.*, without gross sliding.

The stress distributions corresponding to these forces can be approximated as[45]

$$\sigma_n = \left(\frac{3N}{2\pi a^3}\right)(a^2 - r^2)^{1/2} \quad [A4]$$

and

$$\sigma_t = \left(\frac{3CN\tan\theta_i}{2\pi a^3}\right)(a^2 - r^2)^{1/2} \quad [A5]$$

where the subscripts n and t denote normal and tangential stresses, respectively; a is the radius of the circle of contact; and r is the radial position within the contact area.

The effective stress at any point in the contact area is given by

$$\sigma_e = (\sigma_n^2 + 3\sigma_t^2)^{1/2} \quad [A6]$$

Using the results of Goldsmith,[45]

$$a^3 = \left(\frac{3\pi}{4}\right)(RN\delta) \quad [A7]$$

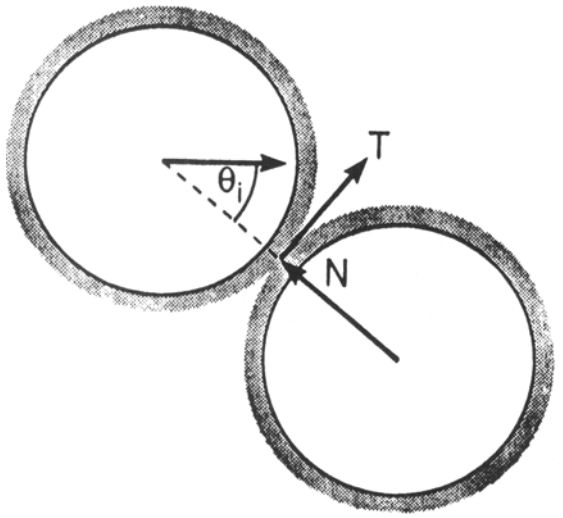

Fig. A1—Two composite balls colliding at an initial impact angle of θ_i produce both normal (N) and tangential (T) components of stress arising from the ball's resistance to deformation.

where $\delta = (1 - \nu^2)/\pi E$, we can write the effective stress as a function of radius in the contact zone:

$$\sigma_e = \left(\frac{2}{\pi^2 R\delta}\right)(a^2 - r^2)^{1/2}(1 + 3C^2 \tan^2 \theta_i)^{1/2} \quad [A8]$$

The development until now holds as long as the composite ball experiences only elastic deformation. However, the powder coating clearly experiences plastic deformation during MA. The onset of this deformation occurs when the effective stress approximately equals the powder hardness (H_v). This occurs first at the center of the contact zone ($r = 0$). The contact radius and the normal approach of the balls at this elastic to elastic-plastic transition are then given by

$$a_{ep} = \left(\frac{\pi^2 R\delta H_v}{2}\right)(1 + 3C^2 \tan^2 \theta_i)^{-1/2} \quad [A9]$$

and

$$\alpha_{ep} = \left(\frac{\pi^4 R\delta^2 H_v^2}{2}\right)(1 + 3C^2 \tan^2 \theta_i)^{-1} \quad [A10]$$

This transition approximately takes place for a value of α on the order of 2 μm.

During the elastic deformation stage, the composite balls have been obeying the equation of motion[45]

$$\frac{1}{2}(\dot{\alpha}^2 - v^2) = -\frac{2}{5}k_1 k_2 \alpha^{5/2} \quad [A11]$$

where $\dot{\alpha}$ is the instantaneous relative velocity of the balls; v is the preimpact velocity; $k_1 = 2/M$, where M is the mass of one ball; and $k_2 = [2R]^{1/2}/3\pi\delta$. If we substitute the value for α_{ep} given by Eq. [A10] into Eq. [A11], we find that $\dot{\alpha}$ is approximately equal to v at the transition. Therefore, the greatest part of the collision duration involves plastic deformation of the powder.

What transpires after the transition from elastic to plastic deformation of the powder is as follows (neglecting any work-hardening of the powder that may take place during the course of the collision). The plastic zone of the powder grows radially, as a circle, with uniform hardness. The corresponding stress distribution has been illustrated in Figure 5. The equations of motion for the composite balls undergoing elastic-plastic deformation can be developed. We assume that the normal forces lead to the stoppage and subsequent separation of the balls. There are two components of the normal force resisting the approach of the balls: the plastic circle surrounding the contact center and the elastic annulus around the plastic zone.

The normal force acting in the plastic zone is given by

$$N_p = \pi r_p^2 H_v \quad [A12]$$

where r_p is the radius of the plastic zone. The normal force in the elastic annulus is

$$N_e = \int_{r_p}^{a} \sigma_n 2\pi r dr \quad [A13]$$

If we assume that outside the plastic zone the stresses given by Eqs. [A4] and [A5] remain valid, the equation of motion of the composite ball is given by

$$\ddot{\beta} + Q\beta = 0 \quad [A14]$$

where

$$\beta = \alpha - \frac{\pi^4 R\delta^2 H_v^2}{6(1 + 3C^2 \tan^2 \theta_i)} \quad [A15]$$

and

$$Q = \frac{\pi R H_v}{M(1 + 3C^2 \tan^2 \theta_i)^{1/2}} \quad [A16]$$

The solutions to Eq. [A14] are

$$\beta = C_1 \sin(kt + C_2) \quad [A17a]$$

$$\dot{\beta} = C_1 k \cos(kt + C_2) \quad [A17b]$$

$$\ddot{\beta} = -C_1 k^2 \sin(kt + C_2) \quad [A17c]$$

where

$$k = \frac{1}{2R}\left[\frac{3H_v}{\rho(1 + 3C^2 \tan^2 \theta_i)^{1/2}}\right]^{1/2} \quad [A18]$$

with ρ being the powder density. For a typical impact in an MA device, k is on the order of 60,000 s^{-1}.

The values of C_1 and C_2 can be determined by use of the initial conditions that at $t = 0$, $\alpha = 0$ and v is the relative impact velocity. We find that over the vast duration of the contact, $kt \gg C_2$, so that we can neglect C_2 in the analysis. On this basis, $C_1 = v \cos \theta_i/k$.

The duration of the compression phase of the collision is

$$\tau = \pi/(2k) \quad [A19]$$

which is approximately 2.5×10^{-5} seconds, or about twice that determined through elastic analysis.[11] Knowing the duration of the compression phase allows us to calculate the final approach of the two composite balls

Table AI. Comparison of Collision Characteristics between Current Model and Previous Model[11]

Parameter	Current Model	Previous Model
Approach (μm)	26	12
Contact radius (μm)	177	199
Strain	0.3	0.28
Impact duration (10^{-5} s)	2.44	1.25

Note: Values of parameters used in calculations are appropriate for a relative collision velocity of 3.9 m/s between balls having a radius of 0.24 cm and a coating thickness of Cu powder equal to 100 μm.

(and hence the deformation of the powder coating them) as

$$\alpha_f = 2Rv \cos \theta_i \left[\frac{\rho(1 + 3C^2 \tan^2 \theta_i)^{1/2}}{3H_v} \right]^{1/2} \quad [A20]$$

We note that this analysis is simplified in that it neglects the effects of tangential force on the collision, apart from the effect this force has on the effective stress. As a result of the tangential force, the balls rotate during the collision, effectively reducing the angle of incidence.[43,46] Nevertheless, the collision time and the maximum approach are dependent on k, and we find that a change in the angle of incidence from 45 to 0 deg results in only a 25 pct change in the value of k.

It is worthwhile to compare the results of the present treatment with a more simplified one we conducted previously.[11] This is done in Table AI; the numerical values listed there are appropriate for the metal Cu having a hardness of 1 GPa. Values for the approach and strain given for the current model are calculated at the contact center; those taken from the previous work are average values in the sense that strain distribution was not considered in the previous model. The radius of the contact calculated on the current model is for plastic deformation only; the real contact radius is slightly greater. Although the two models offer comparable results, the current model provides several advantages. For example, the effect of powder hardness, which changes with processing, is incorporated into this model.

APPENDIX B: PARTICLE DEFORMATION AS A FUNCTION OF POSITION

The deformation of individual particles significantly influences their coalescence and fragmentation proclivities. In this Appendix, we summarize our method for calculating the deformation of the particles based on their geometry and the overall deformation of the composite ball.

Consider two oblate spheroids in contact, as depicted in Figure B1. When these bodies are pressed together, the greatest displacement occurs at the center of contact, and the amount of displacement decreases as we move away from the center. It is necessary to determine this variation in displacement in order to subsequently determine strain as a function of position. In a vertical section (Figure B1), the spheroids are ellipses and the plane defining their contact area is a line. It is a simple matter

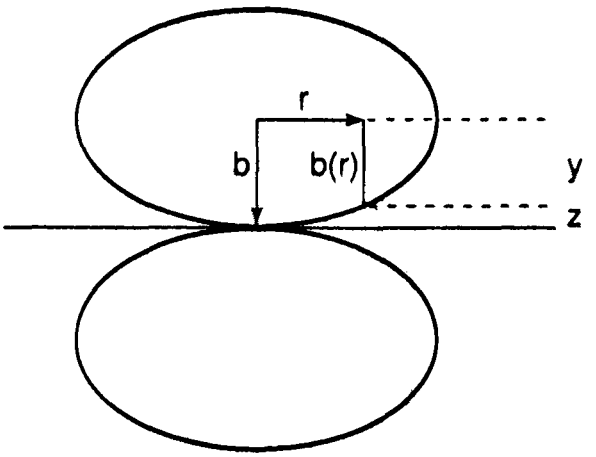

Fig. B1—Deformation of particles along the contact radius between them can be determined by considering the geometry of two oblate spheroids (ellipses in two dimensions) in contact.

to find the distance from any point on the perimeter of this ellipse to this line, and hence to determine the difference in displacement as a function of radial position in the oblate spheroid. The equation for an ellipse is

$$\frac{x^2}{c^2} + \frac{y^2}{b^2} = 1 \quad [B1]$$

Rearrangement of Eq. [B1] provides an expression for y, the vertical distance of Figure B1. The difference in displacement (distance of a point on the surface from the plane) is $z = b - y$, which is obtained as

$$z = b \left[1 - \left(1 - \frac{x^2}{c^2} \right)^{0.5} \right] \quad [B2]$$

We will define the strain at any point by

$$\varepsilon = -\ln \left[\frac{b(r) - \left[\left(\frac{\alpha_p(r)}{2} \right) - z(r) \right]}{b(r)} \right] \quad [B3]$$

where $\alpha_p(r)$ is the approach between homologous points on two particles being pressed together. Since $b(r) = b(0) - z(r)$, and recognizing that

$$\frac{\alpha_p(0)}{2b(0)} = \frac{\alpha}{h_0} \quad [B4]$$

the strain becomes

$$\varepsilon_z(r) = -\ln \left\{ \frac{\left(1 - \frac{\alpha}{h_0} \right)}{\left[1 - \frac{z(r)}{b_0} \right]} \right\} \quad [B5]$$

ACKNOWLEDGMENTS

This work was supported by DARPA/NASA and ARO. Helpful discussions with Professor Doris

Kuhlman-Wilsdorf, Dr. David Makel, and Professor Richard Gangloff are acknowledged.

REFERENCES

1. M.F. Ashby: *Acta Metall.*, 1974, vol. 22, pp. 275-89.
2. E. Artz, M.F. Ashby, and K.E. Easterling: *Metall. Trans. A*, 1983, vol. 14A, pp. 211-21.
3. A. Mortensen, L.J. Masur, J.A. Cornie, and M.C. Flemings: *Metall. Trans. A*, 1989, vol. 20A, pp. 2535-47.
4. C.G. Levi: *Metall. Trans. A*, 1988, vol. 19A, pp. 699-708.
5. U. Mitra and T.W. Eagar: *Metall. Trans. B*, 1991, vol. 22B, pp. 73-81.
6. T. Zacharia, S.A. David, J.M. Vitek, and H.G. Krauss: *Metall. Trans. B*, 1991, vol. 22B, pp. 243-57.
7. F.B. Swinkels and M.F. Ashby: *Acta Metall.*, 1981, vol. 29, pp. 259-81.
8. M.F. Ashby: *HIP 6.0 Users Manual*, Cambridge University Press, Cambridge, England, 1990, pp. 1-70.
9. P.S. Gilman and J.S. Benjamin: *Ann. Rev. Mater. Sci.*, 1983, vol. 13, pp. 279-300.
10. J.S. Benjamin: *Sci. Am.*, 1976, vol. 234 (5), pp. 40-48.
11. D.R. Maurice and T.H. Courtney: *Metall. Trans. A*, 1990, vol. 21A, pp. 289-303.
12. T.H. Courtney and D.R. Maurice: in *Solid State Powder Processing*, A.H. Clauer and J.J. deBarbadillo, eds., TMS, Warrendale, PA, 1990, pp. 3-19.
13. T.H. Courtney, J.C. Malzahn Kampe, J.K. Lee, and D.R. Maurice: in *Diffusion Analysis and Applications*, A.D. Romig and M.A. Dayananda, eds., TMS, Warrendale, PA, 1989, pp. 225-53.
14. R.W. Rydin, D. Maurice, and T.H. Courtney, *Metall. Trans. A*, 1993, vol. 24A, pp. 175-85.
15. B.J.M. Aikin, D.R. Maurice, and T.H. Courtney: *Mater. Sci. Eng.*, 1991, vol. A147, pp. 229-37.
16. B.J.M. Aikin and T.H. Courtney: *Metall. Trans. A*, 1993, vol. 24A, pp. 647-57.
17. G.B. Schaffer and P.G. McCormick: *Metall. Trans. A*, 1992, vol. 23A, pp. 1285-90.
18. R.M. Davis, B.T. McDermott, and C.C. Koch: *Metall. Trans. A*, 1988, vol. 19A, pp. 2867-74.
19. R.B. Schwarz and C.C. Koch: *Appl. Phys. Lett.*, 1986, vol. 49, pp. 146-48.
20. G. Martin and E. Gaffet: *J. Phys. France (Colloq.)*, 1990, vol. 51, pp. C4-9.
21. D. Maurice: Ph.D. Thesis, University of Virginia, Charlottesville, VA, 1992.
22. T. Kosmac, D. Maurice, and T.H. Courtney: *J. Am. Ceram. Soc.*, in press.
23. P.S. Gilman and J.S. Benjamin: *Ann. Rev. Mater. Sci.*, 1983, vol. 13, pp. 279-300.
24. J.J. deBarbadillo and J.H. Weber: Inco Alloys International, Huntington, WV, private communication, 1988.
25. C.W. Thurston and H.J. Deresiewicz: *J. Appl. Mech.*, 1959, vol. 26, pp. 251-58.
26. J. Gil Sevillano, P. van Houtte, and E. Aeronouldt: *Prog. Mater. Sci.*, 1980–81, vol. 25, pp. 69-412.
27. N. Bay: *Met. Constr.*, 1986, vol. 18, pp. 369-74.
28. N. Bay: *Weld. J.*, 1983, vol. 62, pp. 137S-42S.
29. N. Bay: *J. Eng. Ind.*, 1979, vol. 101, pp. 121-27.
30. H.A. Mohamed and J. Washburn: *Weld. J.*, 1975, vol. 54, pp. 302S-10S.
31. S.B. Ainbinder and A.S. Prancs: *Wear*, 1966, vol. 19, pp. 209-27.
32. L.R. Vaidyanath, M.G. Nicholas, and D.R. Milner: *Br. Weld. J.*, 1959, vol. 6, pp. 13-19.
33. J. Robertson and M.I. Manning: *Mater. Sci. Technol.*, 1990, vol. 6, pp. 81-91.
34. L. Nybourg: *Met. Powder Rep.*, 1989, vol. 4 (1), pp. 32-34.
35. V.P. Antipin, V.A. Danilkin, V.A. Sidorov, S.Y. Kabanov, and N.V. Larin: *Poroshk. Metall.*, 1984, vol. 8 (260), pp. 4-9.
36. R.F. Tylecote, D. Howd, and J.E. Furmidge: *Br. Weld. J.*, 1958, vol. 5, pp. 21-38.
37. B. Avitzur: *Metal Forming: Processes and Analysis*, R.E. Kreiger Co., Huntington, NY, 1979, pp. 77-150.
38. P.W. Lee and H.A. Kuhn: *Metall. Trans.*, 1973, vol. 4, pp. 969-74.
39. Y. Bai and B. Dodd: *Res Mech.*, 1985, vol. 13, pp. 227-41.
40. J.W. Hutchinson: *J. Appl. Mech.*, 1983, vol. 50, pp. 1042-51.
41. W.A. Logsdon: in *STP 590*, ASTM, Philadelphia, PA, 1976, pp. 43-58.
42. J.P. Andrews: *Phil. Mag.*, 1930, vol. 9, pp. 593-610.
43. I.V. Maw: *Wear*, 1976, vol. 38, pp. 101-14.
44. R.D. Mindlin: *J. Appl. Mech.*, 1949, vol. 71, pp. A259-68.
45. W. Goldsmith: *Impact*, E. Arnold, London, 1960, pp. 82-98.
46. D. Halliday and R. Resnick: *Fundamentals of Physics*, John Wiley & Sons, New York, NY, 1966, pp. 190-93.